frontiers | Frontiers in Earth Science

TYPE Original Research
PUBLISHED 23 August 2023
DOI 10.3389/feart.2023.1250640

OPEN ACCESS

EDITED BY
Gang Rao,
Southwest Petroleum University, China

REVIEWED BY
Yangwen Pei,
China University of Petroleum, China
Weitao Wang,
Sun Yat-sen University, China

*CORRESPONDENCE
Zhaojie Guo,
zjguo@pku.edu.cn

RECEIVED 30 June 2023
ACCEPTED 14 August 2023
PUBLISHED 23 August 2023

CITATION
Yang Y, Wang Z, Liu R, Peng L, Zhang C and Guo Z (2023), Evolution of kinematic transformation from the Altyn Tagh fault to the Qilian Shan in the northern Tibetan Plateau: from early Cenozoic initiation to mid-Miocene extrusion.
Front. Earth Sci. 11:1250640.
doi: 10.3389/feart.2023.1250640

Evolution of kinematic transformation from the Altyn Tagh fault to the Qilian Shan in the northern Tibetan Plateau: from early Cenozoic initiation to mid-Miocene extrusion

Yizhou Yang[1], Zhendong Wang[1,2], Runchao Liu[1,3], Luying Peng[1], Changhao Zhang[4] and Zhaojie Guo[1]*

[1]Key Laboratory of Orogenic Belts and Crustal Evolution, Ministry of Education, School of Earth and Space Sciences, Peking University, Beijing, China, [2]Petroleum Exploration and Production Research Institute, Sinopec, Beijing, China, [3]Institute of Energy, Peking University, Beijing, China, [4]Qinghai Oilfield Company, PetroChina, Dunhuang, Gansu, China

The Altyn Tagh fault has been a crucial tectonic boundary of the Tibetan Plateau during the Cenozoic India-Eurasia collision. However, issues have not been addressed regarding the Cenozoic evolution of the kinematic transformation from the eastern Altyn Tagh fault to the Qilian Shan. Here we focus on the kinematics at a crucial point, the Subei triple junction, along the Altyn Tagh fault, which was recorded by faulting in the Suganhu basin to the south of the junction. We reconstructed the structural pattern of faults and thickness distribution of the Cenozoic strata in the Suganhu basin by integrating seismic profiles, well logging, and topographic data. We inferred that only crustal shortening and thickening in the Danghenan Shan, a prominent topographic high, absorbed the strike-slip displacement along the Altyn Tagh fault during the early Cenozoic. Since the mid-Miocene, strike-slip fault belts within the Suganhu basin were initiated, based on the fault geometry and uneven thickness distribution across the fault belts. We thus proposed a mid-Miocene kinematic transformation realized by blocks extruding southeastward, as well as the crustal shortening and thickening in the entire Qilian Shan. Those blocks are bounded by preexisting weaknesses with lateral movements, and lithospheric heterogeneity played an essential role in the block-scale extrusion.

KEYWORDS

Suganhu basin, Altyn Tagh fault, Qilian Shan, strike-slip fault, kinematic transformation, northern Tibetan Plateau, triple junction, positive flower structure

1 Introduction

The left-lateral Altyn Tagh fault (ATF) runs along the northern tectonic boundary of the Tibetan Plateau since the India-Eurasia collision (Yin et al., 2002; Molnar and Dayem, 2010). A series of NW-striking fault belts in the Qilian Shan merge into the eastern segment of the ATF. These are fold-and-thrust belts that exhibit minor left-lateral slip near the AFT (Figure 1A; Meyer et al., 1998; Luo et al., 2020). New geodetic

and geomorphological studies have revealed a decrease in the late Quaternary and present-day strike-slip rates along the eastern segment of the ATF, ranging from ca. 10 mm/yr near the Aksay bend (93–94 °E) to 0 mm/yr in the Jiuxi basin (97–98 °E) (Figure 1B; e.g., Zhang et al., 2007; Wu et al., 2019; Liu et al., 2020). Given the tectonic patterns along the eastern segment of the ATF, it is expected that the decreasing strike-slip rates ought to be accommodated by the deformation within the Qilian Shan (Meyer et al., 1998; Van der Woerd et al., 2001).

However, consensus has not been reached regarding the transformation of the strike-slip displacement from the ATF to the Qilian Shan. Most researchers focused on NE-SW directed continuous crustal shortening and thickening resulting from folding and thrusting in the Qilian Shan (Zhang et al., 2007;

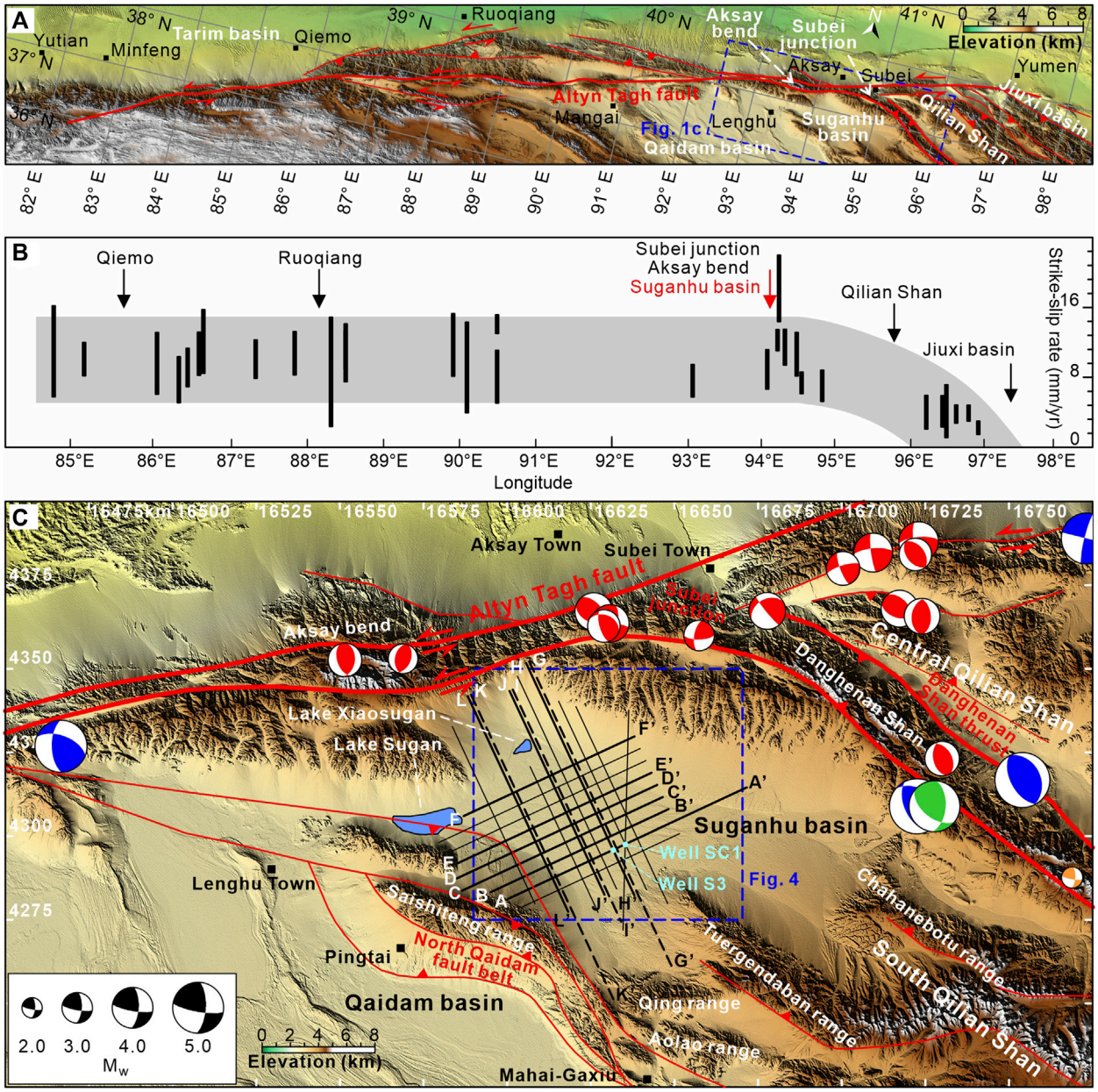

FIGURE 1
(A) Structural map of the Altyn Tagh fault system and the Qilian Shan fold-and-thrust belt. The Subei junction represents an initial transformation from the Altyn Tagh fault to the Qilian Shan. **(B)** Present and late Quaternary left-lateral strike-slip rates along the Altyn Tagh fault, modified after Wu et al. (2019) and Zhang et al. (2007). Black bars represent values of strike-slip rates with errors (see references in Wu et al. (2019) for their sources). Note that the Subei junction along with the Suganhu basin marks a crucial point where the strike-slip rate along the Altyn Tagh fault starts to decrease eastward. **(C)** Topographic and structural maps of the Suganhu basin and the Subei junction (6-degree Gauss-Krüger map projection). Red lines denote faults with either reverse faulting (marked by red triangles) or left-lateral strike-slip (marked by two red arrows). Beach balls along the Altyn Tagh fault and Danghenan Shan thrust are focal mechanism solutions given by Pan et al. (2020) (red), Molnar and Lyon-Caent (1989) (green), GCMT (www.globalcmt.org; blue), and Han et al. (2019) (orange). Radius of the beach balls is scaled with the value of moment magnitude. Solid back lines denote seismic profiles, whereas dashed black line denotes a topographic profile. Sky blue points are drill wells in the Suganhu basin.

Zheng et al., 2013; Zhang et al., 2014). However, others argued that the amount of shortening in the Qilian Shan is insufficient to absorb the total displacement along the ATF (e.g., Cheng et al., 2019b). For instance, Xu et al. (2005) conducted kinematic analyses at triple junctions along the eastern segment of the ATF and predicted the occurrence of additional extension or lateral movements parallel to the fault belts in the Qilian Shan. Cheng et al. (2015b) also suggested an extra eastward extrusion in the Qilian Shan, based on the disparity between the crustal shortening in the Qilian Shan (250 ± 28 km) and the total Cenozoic displacement along the ATF (360 ± 40 km). Poor understandings of the kinematics of the Altyn Tagh fault movements in the Qilian Shan region hinder our ability to assess this transformation.

The second puzzle is when and where the kinematic transformation initiated along the ATF, corresponding to the Cenozoic growth in the Qilian Shan. Early studies suggested that the Qilian Shan, as the northern front of the Tibetan Plateau, has gradually grown northward since the Miocene (Tapponnier et al., 2001). Given a growing number of studies in low-temperature thermochronology, provenance analyses, and tectonic modeling, an alternative viewpoint suggested that the Qilian Shan has bidirectionally expanded from its center to the north and south since the Miocene (Zheng et al., 2017; Pang et al., 2019a; Zhang et al., 2022). On the contrary, other researchers have emphasized the importance of early Cenozoic growth activities in the Qilian Shan region. Some argued that the South Qilian Shan began its exhumation in the Paleogene to Early Eocene and the topographic growth has accelerated throughout the Qilian Shan since the middle to late Miocene (He et al., 2022; Li et al., 2022). Other studies even proposed that tectonic activities have occurred following an "out of sequence" pattern in the Qilian Shan region since the early Cenozoic (Yin et al., 2008; Zuza et al., 2018; Li et al., 2019; Wu et al., 2021). These disagreements lead to chaotic understandings of not only the transformation evolution of the eastern ATF but also the growth of the northern Tibetan Plateau.

The Subei junction marks a clockwise veering from the ENE striking ATF to the SE striking Danghenan Shan thrust (one of the fault belts in the Qilian Shan; Figure 1C). It serves as a point where the strike-slip rates along the ATF start to decrease eastward (Figure 1B; Xu et al., 2005; Zhang et al., 2007). This junction not only accommodates nearly half (ca. 5 mm/yr) of the total strike-slip rates along the ATF but also corresponds to the most rapid drop of the strike-slip rates (~9.8 mm/yr/100 km near the junction, compared to 2.5 mm/yr/100 km to the east of the junction), providing an excellent site for investigating the kinematic transformation between the eastern segment of the ATF and Qilian Shan (Liu et al., 2020). Located at the southern corner of the Subei junction, the Suganhu basin filled with Cenozoic deposits preserves a long-term record of the syn-sedimentary deformation of the Subei junction (Figure 1C; Cheng et al., 2019b). Based on seismic profiles, well logging, and topographic data, here we aim to reconstruct the structural pattern of faults and the thickness distribution of the Cenozoic strata in the Suganhu basin to decipher the evolution of the kinematic transformation from the eastern segment of the ATF to the Qilian Shan.

2 Geological setting

2.1 Altyn Tagh fault

The Altyn Tagh fault (ATF) is an ENE-striking lithospheric fault that stretches over a distance of 1,600 km, starting from the western Kunlun Shan and terminating in the Jiuxi basin (Figure 1A). It accommodated one-third of the India-Eurasia convergence through left-lateral faulting during the Cenozoic (Avouac and Tapponnier, 1993; Wittlinger et al., 1998; Yin and Harrison, 2000; Cowgill et al., 2003; Zhang et al., 2004; Zhao et al., 2006; Zhang et al., 2021). Extensive studies have documented a substantial Cenozoic displacement of ca. 350–500 km along the ATF (Ritts and Biffi, 2000; Yue et al., 2001; Chen et al., 2002; Yin et al., 2002; Cowgill et al., 2003; Ritts et al., 2004; Yue et al., 2005; Cheng et al., 2015a). The timing of Cenozoic strike-slip faulting along the ATF has been a subject of ongoing debate, ranging from the Paleogene to the middle Miocene, yet most studies supported a scenario of mid-Miocene accelerated lateral faulting of the ATF, accompanied by an intensified growth of mountain range (Jolivet et al., 2001; Cowgill et al., 2004; Sun et al., 2005; Wang et al., 2006; Zhuang et al., 2011; Zhang et al., 2014; Wang et al., 2016a; Cheng et al., 2016; Zhang et al., 2018; Yu et al., 2019b; Wu et al., 2019; Gao et al., 2022; Zeng et al., 2023). The ATF exhibits geometric complexities, including bends and oblique splays along its eastern segment. The bends, such as the Aksay bend, form restraining positive flower structures bounded by two steep lithospheric faults (Elliott et al., 2015; Xiao et al., 2017), and the splays represent triple junctions, such as the Subei junction which involves in kinematic transformations of the strike-slip displacement (Figure 1C; Meyer et al., 1998; Van der Woerd et al., 2001; Xu et al., 2005).

2.2 Qilian Shan and Danghenan Shan thrust

The Qilian Shan, with elevations exceeding 4,000 m, forms the northeastern periphery of the Tibetan Plateau and is situated between the Qaidam and Jiuxi basins (Figure 1A). This mountainous region consists of subparallel NW-SE striking active fold-thrust belts inherited from preexisting weaknesses (Zuza et al., 2018). The northwestern termination of these belts into the ATF indicates that the observed shortening in the Qilian Shan is a response to the decreasing eastward strike-slip rates along the ATF (Meyer et al., 1998; Van der Woerd et al., 2001; Zhang et al., 2007; Cheng et al., 2015b). However, some studies have proposed that the formation of the Qilian Shan is a direct consequence of the collision between the Eurasia and India continents (Allen et al., 2017). Regarding its Cenozoic tectonic evolution, the Qilian Shan has experienced rapid growth since the mid-Miocene (George et al., 2001; Bush et al., 2016; Wang et al., 2017b; Pang et al., 2019a; Nie et al., 2020; Lu et al., 2022b; Yu et al., 2023). Moreover, some studies have suggested an early Cenozoic initiation of growth in the Qilian Shan, highlighting its far-field response to the continental collision (Jolivet et al., 2001; Zhuang et al., 2011; Jian et al., 2018; Cheng et al., 2019a; Lu et al., 2019; An et al., 2020; Song et al., 2020; He et al., 2022).

The Danghenan Shan thrust, an active structural belt branching from the Subei junction, extends over a distance of 250 km in the

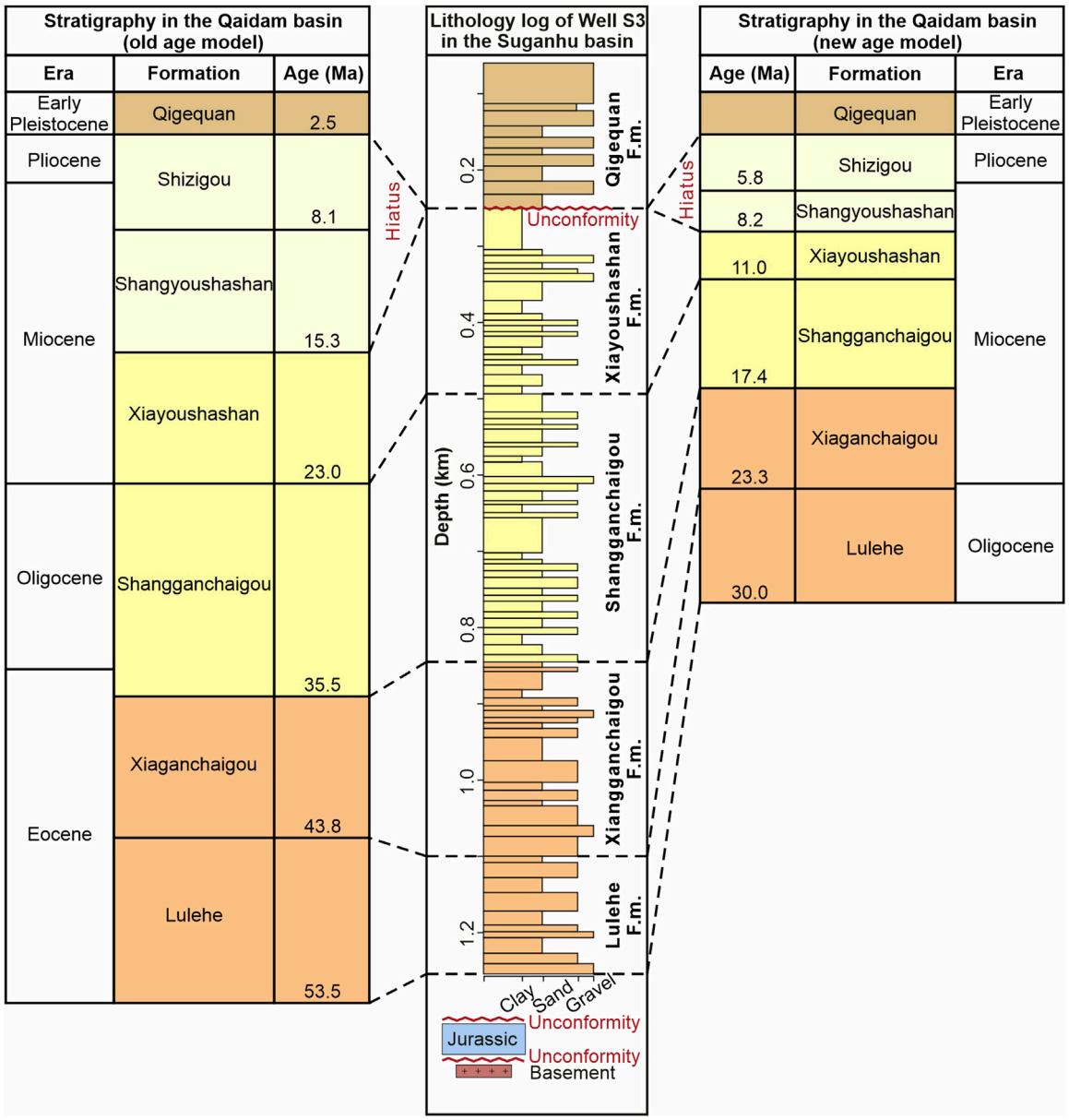

FIGURE 2
Lithology log of Well S3 represents the Cenozoic stratigraphic framework in the Suganhu basin, modified after Cheng et al. (2019b). See Figure 1C for the location of Well S3. Note that the Cenozoic stratigraphies in the Suganhu and the Qaidam basins share the same age model (ages compiled after Ji et al. (2017) and Wang et al. (2017b)).

South Qilian Shan and defines the boundary of the Danghenan Shan as a prominent topographic high (Figure 1C; Meyer et al., 1998; Shao et al., 2017; Xu et al., 2021). During Cenozoic deformation along the northern piedmont of Danghenan Shan thrust, Paleozoic granitic plutons and metasedimentary rocks, which form the core of the Danghenan Shan, were emplaced onto the Neogene red beds and Pleistocene fluvial-alluvial strata (Meyer et al., 1998; Van der Woerd et al., 2001; Yi et al., 2022). This emplacement also resulted in cutting and folding of sediments and fluvial terraces near the frontal fault scarps (Shao et al., 2017). Similar to the Qilian Shan, the Danghenan Shan also underwent significant growth since the middle Miocene, as evidenced by rapid exhumation within the range and coarsening-upward sequences in nearby basins (Yin et al., 2002; Wang et al., 2003; Sun et al., 2005; Lin et al., 2015; Zhuang et al., 2018; Yu et al., 2019b). Recent studies have reported an initiation of exhumation from the late Paleocene-early Eocene to the Oligocene, predating the mid-Miocene rapid exhumation stage (Yin et al., 2002; Li et al., 2017; He et al., 2020; Feng et al., 2022; He et al., 2022).

2.3 Suganhu basin

The Suganhu basin, the largest depression in the Qilian Shan, is bordered by the ATF to the northwest, the Danghenan Shan thrust

to the northeast, the Saishiteng range to the southwest, and the Chahanebotu, Tuergendaban, and Qing ranges of the Qilian Shan to the southeast (Figure 1C; Cheng et al., 2019b). The modern Suganhu basin is nearly dried out and thus leaves two lakes near the ATF called Lake Sugan to its west and Lake Xiaosugan to its northwest (Figure 1C). Unlike those long, narrow, and linear intermountain basins induced by internal shortening in the Qilian Shan (Zhang et al., 2014), the present-day Suganhu basin has an equidimensional shape in the map view. Subsurface reflections indicate that the interior Suganhu basin is characterized by high-angle basement-involved faults and related folds (Cheng et al., 2019b; Cheng et al., 2019c).

Previous stratigraphic studies have revealed that the Suganhu basin is filled with Cenozoic terrestrial deposits, reaching a total thickness of up to 3 km and shares a similar sequence-stratigraphic framework with the Qaidam basin (Meng and Fang, 2008; Cheng et al., 2019b). However, there has been controversy regarding the age model of the Cenozoic sequence in the Qaidam and Suganhu basins (Figure 2). Some researchers support an old age model, suggesting that the first Cenozoic sediments had not deposited until the early Eocene (Zhang, 2006; Ke et al., 2013; Ji et al., 2017). Conversely, others argue for an Oligocene-to-Middle-Miocene initiation of the sediment accumulation, known as the new age model (Wang et al., 2017b; Nie et al., 2020; Lu et al., 2022a; Duan et al., 2022; Wang et al., 2022). By integrating fossil correlation between the Suganhu and Qaidam basins, well logging, and the old age model, the Cenozoic sequence in the Suganhu basin is subdivided into five units: 1) the Lulehe F.m. (early Eocene, 53.5-43.8 Myr), 2) Xiaganchaigou F.m. (late Eocene, 43.8-35.5 Myr), 3) Shangganchaigou F.m. (Oligocene, 35.5-23.0 Myr), 4) Xiayoushashan F.m. (mid-Miocene, 23.0-15.3 Myr), and 5) Qigequan F.m. (early Pleistocene, <2.5 Myr), in geochronological order from the oldest to the youngest (Meng and Fang, 2008; Wu et al., 2019; Hu et al., 2022). Note that the Lulehe F.m. unconformably overlies the lower basement rock or Jurassic deposits, and a mid-Miocene to Pliocene sedimentary hiatus corresponds to the unconformity between the Qigequan and Xiayoushashan F.m. (Figure 2). These strata provide constraints on the deformation history of the basement-involved faults in the Suganhu basin, which are considered to have been activated during the early Cenozoic (Cheng et al., 2019b).

3 Materials and methods

The subsurface structures in the study area were reconstructed and analyzed using seismic data. A total of seventeen 2D pre-stack time-migration seismic profiles were utilized, covering almost the entire Suganhu basin with an area of ca. 3,700 km^2 (Figure 1C). The original seismic data in SEG-Y format were acquired from the Qinghai Oilfield Company, PetroChina. Among these seismic profiles, eight profiles extend from the ATF to the southeastern Suganhu basin in a S25°E direction, while nine profiles run N65°E from the Saishiteng range to the Danghenan Shan (Figure 1C). To interpret and model the subsurface structures, the seismic profiles were imported into the IHS Kingdom (SMT) software. By analyzing the offsets of seismic events within the profiles, the traces and apparent separation of subsurface faults were delineated. The tops of the Cenozoic formations were determined in time-domain using synthetic seismograms and previous borehole records from a referenced well, SC1 (Figure 1C). Horizon lines were interpreted following lateral tracking of seismic reflections from Well SC1's marked formation tops and closed at the intersections between different seismic profiles. Subsequently, 3D meshes of fault system and horizons were generated by interpolating the interpreted fault traces and horizon lines. Intersection lines between the meshes of fault and horizon (bottom of the Cenozoic deposits) were projected to the surface in the Suganhu basin, making up the fault-distribution map. Additionally, specific patterns of seismic reflection termination, such as onlap, were targeted to reconstruct the evolution of range growth. A comparison between the interpreted seismic and topographic profiles is introduced to determine shifts of the depocenter in the Suganhu basin from the early Cenozoic to the present.

Time-to-depth conversion was applied to generate the thickness distribution map. Subsurface seismic velocity was approximated using the acoustic logs from Well S3 and SC1. The relationship between two-way travel time and depth was determined by the equation:

$$\Delta T = 2 \times 10^{-3} AC\,\Delta D$$

where ΔD represents the differential of true vertical depth with respect to the sampling interval of well logging m), ΔT denotes the differential of two-way travel time (ms), and AC denotes the acoustic log (μs/m). A time-depth table was constructed using summation. Subsequently, we employed the quadric polynomial and the least square method to accurately fit the time-depth table as:

$$D = a\,T^2 + b\,T + c$$

where D denotes the true vertical depth m), T denotes the two-way travel time (ms), and a, b, and c are the coefficients of quadric polynomial. The time-depth table was utilized to transform the 3D formation tops into the depth-domain, ensuring accurate depth information. Perpendicular lines were then constructed between the formation tops to generate the thickness distribution map around the referenced wells.

4 Results and interpretations

4.1 Geometry of subsurface fault system

4.1.1 Description

Here we present the observed subsurface structures in the Suganhu basin by integrating seismic data interpretation and 3D modeling. Our analyses reveal five fault belts, namely the East Huahaizi (EHHZ), Huahaizi (HHZ), East Huangyangtan (EHYT), Huangyangtan (HYT), and North Saishiteng (NSST), arranged from northeast to southwest (Figure 3).

The NNW-striking EHHZ fault belt is bounded by two steep faults that dip in opposite directions (Figure 3). These boundary faults converge downward into one major fault rooted in the basement, composing an asymmetric positive flower structure. The Eocene strata (Lulehe and Xiaganchaigou F.m.) and Oligocene to early Miocene strata (Shangganchaigou and Xiayoushashan F.m.) are tilted and cut by the EHHZ fault belt, while the Quaternary strata (Qigequan F.m.) are only cut in the northwestern Suganhu basin (profiles EE' and FF') and slightly

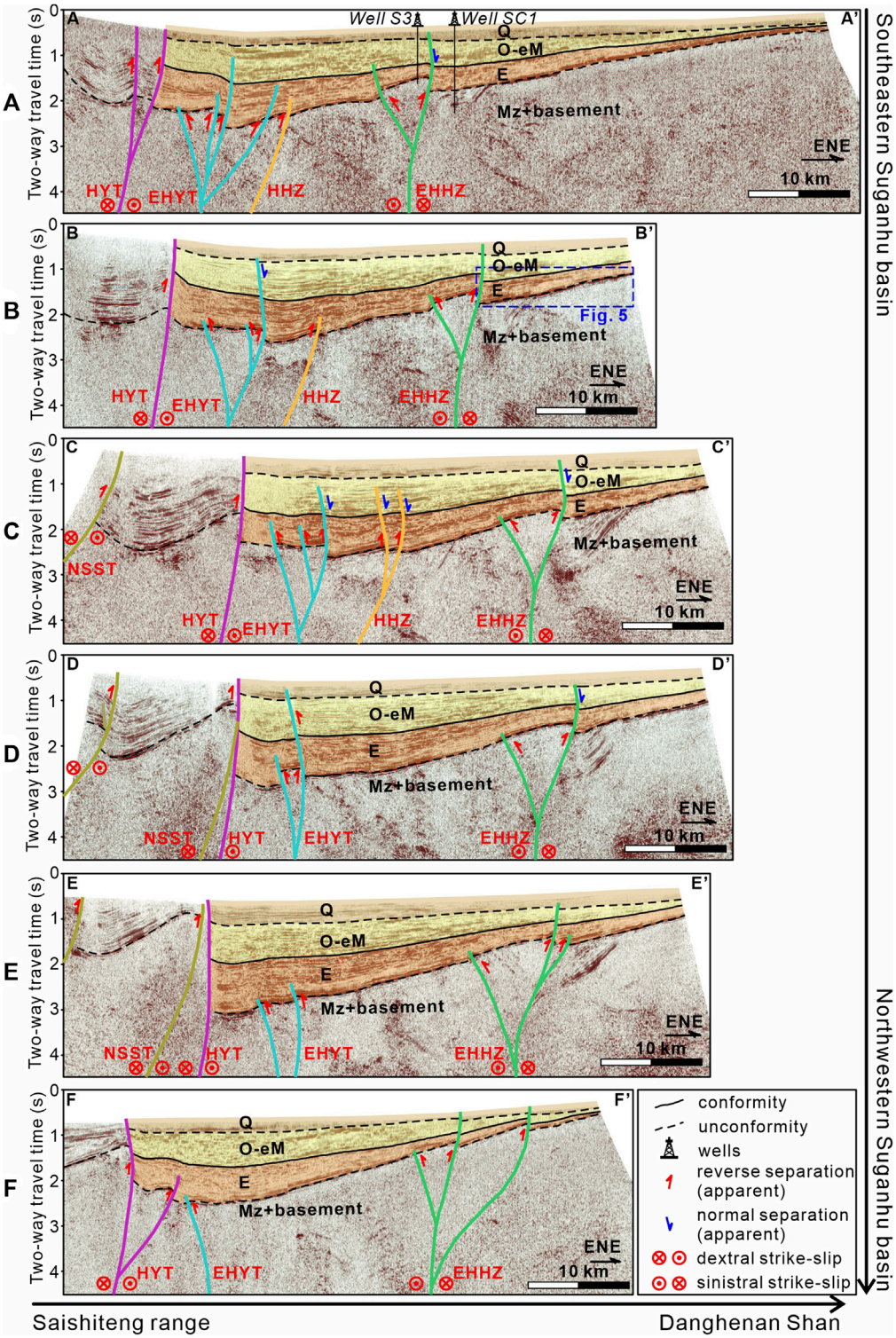

FIGURE 3
ENE-striking seismic profiles revealing the subsurface structures in the Suganhu basin (see Figure 1 for locations). **(A–F)** Seismic profiles AA′ to FF′ from the southeastern Suganhu basin to the northwest. The brown, purple, sky blue, orange, and green lines denote five interpreted fault belts in the basin (faults belt EHHZ for East Huahaizi, HHZ for Huahaizi, EHYT for East Huangyangtan, HYT for Huangyangtan, and NSST for North Saishiteng). The arrows near the faults represent apparent moving directions of the hanging wall, and the red and blue arrows indicate reverse and normal separation of the faults, respectively. The red circle with a dot inside denotes movement going out of the screen, while the red circle with a cross inside denotes movement going into the screen. The colored and translucent polygons are Cenozoic strata (code Q for Quaternary, O for Oligocene, eM for early Miocene, E for Eocene, and Mz for Mesozoic). The solid black lines denote conformable horizons between the Oligocene-to-early-Miocene and Eocene deposits, while the dashed denote unconformities running along the bottom of the Quaternary and Eocene strata.

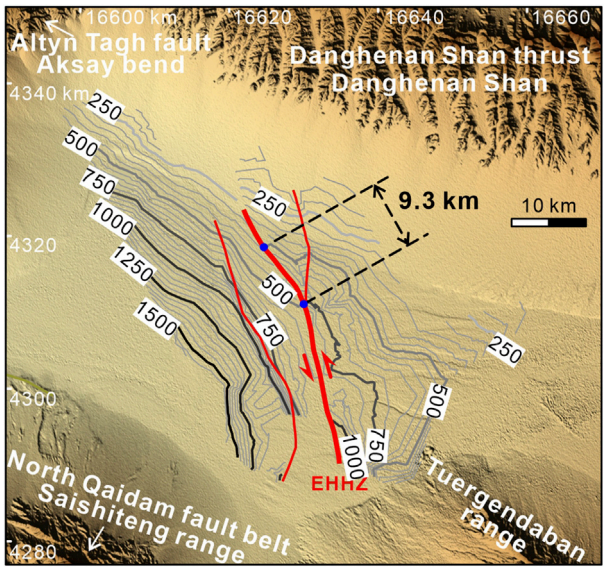

FIGURE 4
Isopach map for the EHHZ (East Huahaizi) fault belt in the Suganhu basin, showing the thickness (meters) of the Eocene deposits (see Figure 1C for location). The 500-m-thick isolines show a 9.3-km left-lateral displacement along the major fault (bold red line) of the EHHZ fault belt. Blue points are the reference points offset by the left-lateral displacement along the EHHZ fault belt.

folded. Although the EHHZ fault belt generally demonstrates reverse separation along its sub-vertical faults, the ENE boundary fault in profile AA' exhibits a curved C-shaped trace characterized by both reverse and normal separation (Figure 3A). The lower part (below 1.2 s in the two-way travel time domain) of this boundary fault dips to the ESE and displays reverse separation of the Eocene strata. Conversely, the upper part (above 1.2 s) changes its dip direction to the ENE with normal separation of the Oligocene to early Miocene strata. The C-shaped trace of the fault, as well as the opposite separation directions at different depths, conform to the definition of the "ribbon effect" proposed by Zolnai (1991). Furthermore, as the flower structure extends northward along its strike, profiles EE' and FF' exhibit more branching faults (Figures 3E, F).

Similarly, the HHZ and EHYT fault belts strike NNW-SSE and are characterized by positive flower structures composed of steep basement-involved faults (Figure 3). Not only the Eocene and Oligocene to early Miocene strata are cut, tilted, and folded by these two fault belts, but also the Quaternary strata are involved in the deformation and displacement induced by the EHYT fault belt. The so-called "ribbon effect" is also observed along the fault belts in profiles BB', CC', and DD' (Figures 3B,C). Significantly, the EHYT fault belt has normal separation of the Oligocene to Quaternary strata in profiles BB and CC', but profile DD' manifests reverse separation along the same branch fault. This along-strike variation of the fault separation corresponds to the "dolphin effect" by Zolnai (1991). Moving from the southeast to northwest, the number of branch faults in the EHYT fault belt decreases along its strike, and the apparent displacement of the HHZ and EHYT fault belts becomes smaller. Specifically, the HHZ fault belt is restricted to the Cenozoic sequence in the southwestern Suganhu basin (Figures 3A–C), disappearing to the northwest (Figures 3D–F).

The NNW-striking HYT fault belt comprises a high-angle major fault and an additional branch fault with reverse separation, cutting through the entire Cenozoic cover and basement in the Suganhu basin (Figure 3). Notably, the major fault also exhibits a C-shaped trace in the profiles DD', EE', and FF' (Figures 3D–F). The apparent displacement of the HYT fault belt reaches its maximum in profile EE' and gradually decreases along its strike from the middle-out (Figure 3E).

Regarding the NSST fault belt, it strikes NNW-SSE but veers counterclockwise to the northwest (Figure 3). It merges with the NNW-striking HYT fault belt to the southeast (Figures 3C–E). In cross-section view, faults within the NSST fault belt exhibit a concave-upward trace cutting through the entire Cenozoic cover, displaying notable throws and fault-related folds (Figures 3E, F). In addition, these faults show lower dip angles of their fault planes compared to other faults in the Suganhu basin (Figures 3C–E).

4.1.2 Interpretation

Our findings suggest that the fault belts, including EHHZ, HHZ, EHYT, and HYT, should be classified as strike-slip faults. Integration of geometric features, such as steep fault planes and flower structures, strongly indicates strike-slip characteristics of these fault belts. Besides, the Cenozoic strata deformed by these faults display only low-amplitude folding in seismic profiles rather than high-amplitude fault-related folding commonly induced by compressional thrusts (Shaw et al., 2005). Compressional thrusting fails to explain the reverse and normal separation along the same faults neither, which are observed not only in different profiles perpendicular to the fault strike but also at varying depths. In contrast, these observed structural patterns, namely the dolphin and ribbon effects, are distinct indicators of strike-slip faults and are associated with the complexities of fault geometry and dip-slip kinematics along the fault strike (Zolnai, 1991; Liu et al., 2017; Liang et al., 2020; Cheng et al., 2022). Therefore, we suggest that it is strike-slip faulting rather than thrusting that dominates these fault belts.

4.2 Tectonic-controlled thickness distribution of the cenozoic strata

4.2.1 Description

Another crucial observation is the uneven thickness distribution of the Cenozoic strata in the Suganhu basin. This unevenness is demonstrated in three aspects presented in the seismic profiles and the thickness distribution map. Firstly, the seismic profiles striking ENE (AA' to FF') exhibit a gradual thickening of the pre-Quaternary strata from the Danghenan Shan toward the Suganhu basin (Figure 3). Taking the Eocene deposits as an example, the isopach map shows that the thickness increases by 250 m every 4.5 km horizontal distance in a basinward direction near the Danghenan Shan (Figure 4). The basinward thickening is also accompanied by seismic events onlapping to the basin-basement toward the Danghenan Shan in cross-section view (Figure 5). In addition, the pre-Quaternary strata maintain a limited thickness of

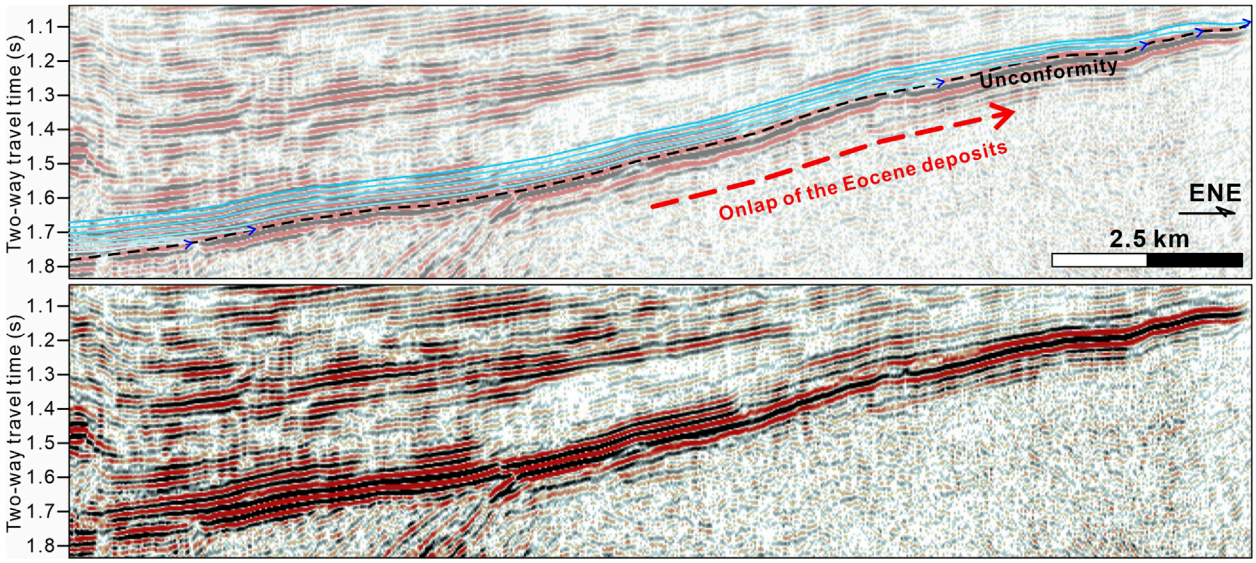

FIGURE 5
Onlaps of the Eocene deposits close to the southern frontal Danghenan Shan in profile BB′ (see Figure 3B for location). Sky blue lines denote seismic events. Dashed black line refers to the unconformity between the Cenozoic cover and Mesozoic deposits or basement rock. Blue arrows are onlap points of the Eocene deposits. Dashed red line denotes a onlap direction of the seismic events.

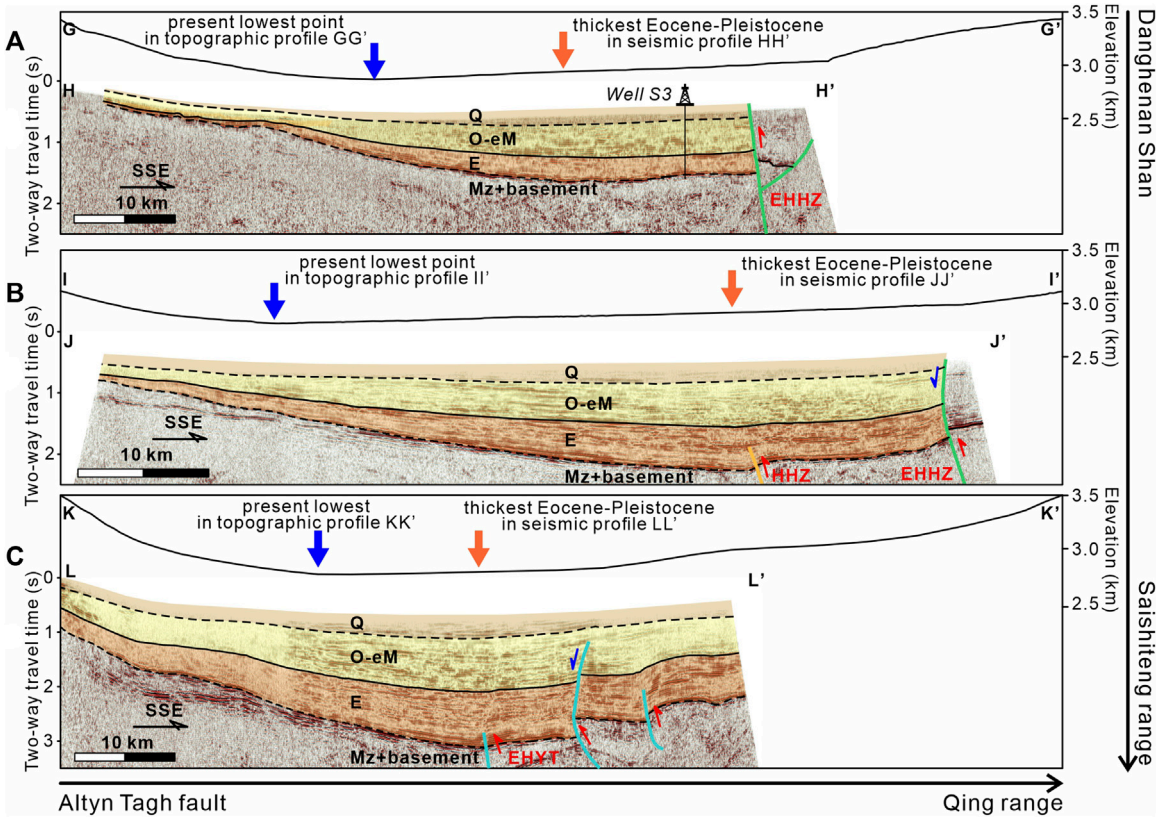

FIGURE 6
(A–C) NWN-striking topographic profiles GG′, II′, and KK′ and their corresponding seismic profiles HH′, JJ′, and LL′ revealing the subsurface structures in the Suganhu basin (see Figure 1 for locations).

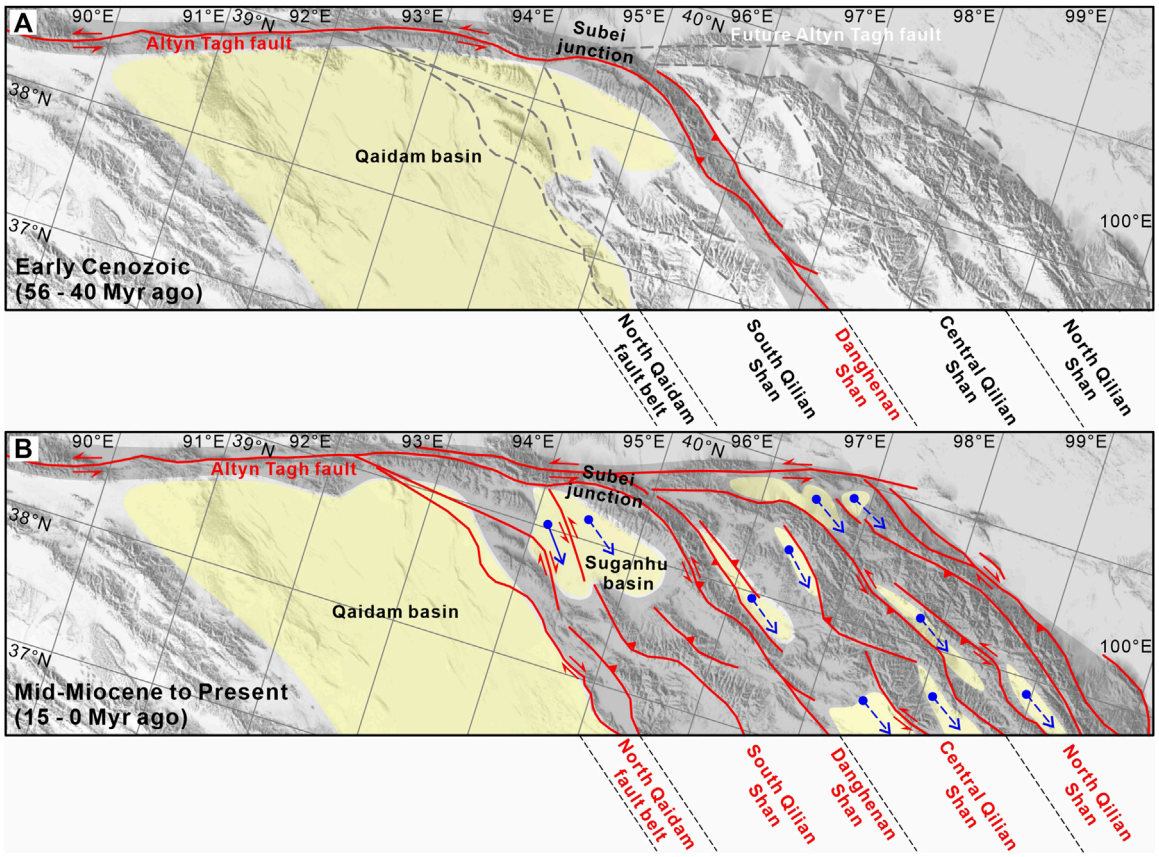

FIGURE 7
(A) Paleogeography and fault distribution in the northern Tibetan Plateau during the early Cenozoic (56–40 Myr ago). Red lines are activated faults, while the dashed grey lines are nonactivated weaknesses. Note that the kinematic transformation from the Altyn Tagh fault is characterized by crustal shortening and thickening in the Danghenan Shan. **(B)** Paleogeography and fault distribution in the northern Tibetan Plateau since the mid-Miocene (15–0 Myr ago). Solid blue arrows represent the southeastward extrusion of the block in the Suganhu basin, while the dashed blue arrows are the inferred block-scale extrusion in the Qilian Shan. Note that the kinematic transformation is absorbed by both extrusion and crustal shortening and thickening in the entire Qilian Shan.

less than 50 m in the seismic profiles AA' and FF' at the southern frontal Danghenan Shan (Figures 3A, F).

The second aspect of unevenness is the abrupt change in thickness of the pre-Quaternary strata across certain fault belts, such as the EHHZ and EHYT. Generally speaking, the hanging-wall thickness is thinner than the footwall in the seismic profiles AA' to FF' (Figure 3). Moreover, strata thickness in the hanging walls and footwalls only shows notable differences in the seismic profile AA' and exhibit a little contrast in the profiles to the northwest (Figure 3).

Lastly, unevenness is also observed within the same faulted wall. For instance, profile AA' display a basinward thickening of the pre-Quaternary strata in the hanging wall of the EHHZ fault belt, which is sandwiched between the two boundary faults of the positive flower structures (Figure 3A).

Furthermore, we notice a mismatch between the present lowest point in the topography of the Suganhu basin and the point of the thickest Cenozoic strata revealed by the seismic profiles. All the topographic profiles, which correspond to the traces of the NNW-striking seismic profiles, exhibit an asymmetric landscape, with a steeper northwestern slope and a gentler southeastern slope of the Suganhu basin (Figure 6). The lowest points in these topographic profiles precisely mark the present Lake Xiaosugan close to the Aksay bend, showing a northward offset from the point of the thickest Cenozoic strata (Figure 6).

4.2.2 Interpretation

The thickness distribution of the Cenozoic strata offers valuable insights into the sedimentary processes which were results of the growth of the Aksay bend and Danghenan Shan, as well as the kinematics and activities of the fault belts in the Suganhu basin.

Based on the basin-scale thickness distribution and sedimentary onlaps, we prefer that the Danghenan Shan should be a topographic high and have experienced gradual uplift since the Eocene. The Danghenan Shan, an early Cenozoic topographic prominent, led to a topographic gradient that is consistent with the basinward thickening tendency in seismic profiles (Figure 3), as well as the isolines aligning parallel to the strike of the Danghenan Shan in the Eocene isopach map (Figure 4). The limited thickness of the Cenozoic strata and onlaps at the southern piedmont of the Danghenan Shan further indicate its long-standing role as a paleogeographical northern boundary for the Suganhu basin throughout the Cenozoic (Figures 3A, F; Figure 5). We attribute

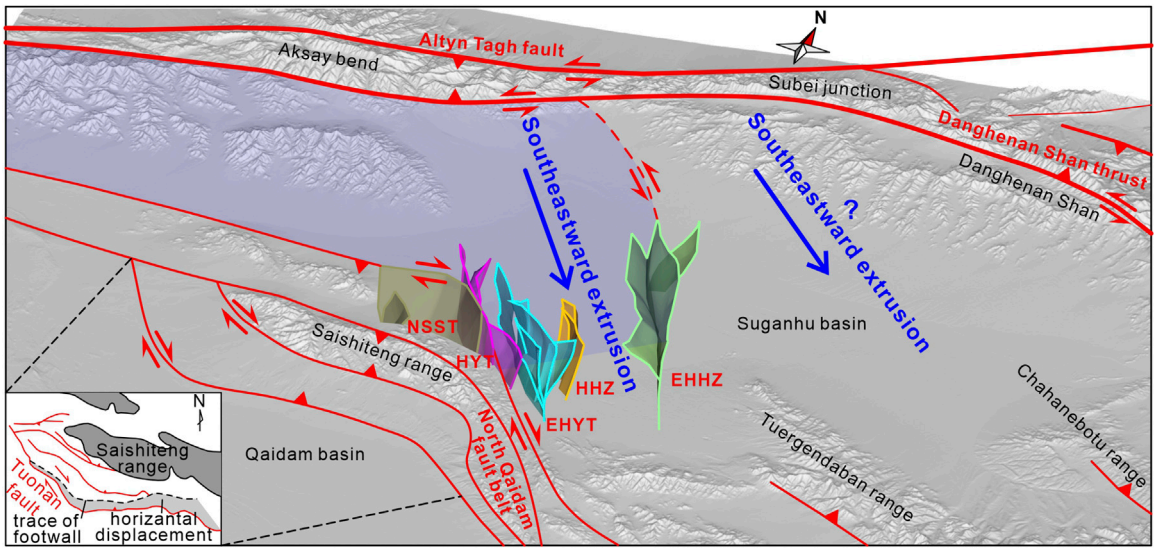

FIGURE 8
A scheme of southeastward block-scale extrusion (pale blue area) in the Suganhu basin. Note the dextral and sinistral strike-slip faulting along the North Qaidam fault belt and EHHZ fault belt, respectively. Subfigure is modified after Xiao et al. (2006) and Mao et al. (2016). Abbreviation of the fault belts in the Suganhu basin: EHHZ for East Huahaizi, HHZ for Huahaizi, EHYT for East Huangyangtan, HYT for Huangyangtan, and NSST for North Saishiteng.

the relatively high altitude of the Danghenan Shan to the synsedimentary uplift since the Eocene, owing to the substantial thickness of Eocene deposits in the Suganhu basin sourced from the Danghenan Shan (Cheng et al., 2019b).

Additionally, we also note a depocenter migration, indicated by the mismatch between the present topographic low and the point of the thickest Cenozoic strata, in cross-section view perpendicular to the ATF (Figure 6). The shift in depocenter could be attribute to the tectonics in the Aksay bend. Continuous growth and uplift of the Aksay bend during the late Cenozoic led to topographic loading and flexural bending of the basement in the Suganhu basin. This process formed an asymmetric landscape similar to the foreland basin system (see DeCelles and Giles, 1996 for its structural pattern), where the topographic low is located at the foredeep close to the piedmont. As a result, the depocenter in the Suganhu basin shifted from a fixed position at the basin's center to the northwest since the late Cenozoic.

Previous studies held a view that the thrust-induced throws since the early Cenozoic resulted in the abrupt thickness change across the fault belts and uneven strata thickness within the same faulted wall, further treated as growth strata (Cheng et al., 2019b). Considering the 3D basin-scale variation of strata thickness, here we prefer an alternative interpretation that the fault belts in the Suganhu basin are strike-slip faults activated since the mid-Miocene. Given the consistent thickening direction from the Danghenan Shan to the Suganhu basin in the ENE-striking seismic profiles, the unevenness within the same faulted wall is consistent with this basin-scale thickening tendency, independent of the dip-directions of the faults (Figure 3). In other words, the unevenness within the same faulted wall could be the result of the growth of the high-altitude Danghenan Shan. Furthermore, thickness distribution map of the Eocene strata shows systematic left-lateral displacement of the isolines along the EHHZ fault. For instance, the displaced isolines of 500-m thickness indicate a left-lateral displacement of 9.3 km along the EHHZ fault belt (Figure 4). We thus attribute the abrupt thickness change across the fault belts is the result of both the Cenozoic strata with spatial variant thickness and strike-slip faulting. It is also important to note that the apparent throws of the Cenozoic bottom along the EHHZ fault belt are ca. 600 m, as documented by Well SC1 in the footwall and Well S3 in the hanging wall. The significant disparity between the apparent throws and lateral displacement supports the dominance of strike-slip faulting rather than thrust faulting alone and highlights the geometric features related to strike-slip faults (mentioned in section 4.2). We infer a possible mid-Miocene initiation for these fault belts in the Suganhu basin, considering the regional unconformity, which is related to the tectonic activities of the fault belts, between the Quaternary and early-Miocene strata (Figure 2).

5 Discussion

Previous transformation models have suggested a disagreement concerning the kinematics in the Qilian Shan. The crustal-shortening-and-thickening model considered the fault belts in the Qilian Shan as thrust faults (Zhang et al., 2007; Zheng et al., 2013). On the other hand, the extrusion model implied additional dextral and sinistral lateral movements along the southern and northern boundary of the Qilian Shan, respectively (Cheng et al., 2015b). Understanding the kinematics in the Qilian Shan is thus crucial in deciphering this transformation.

The second issue is that previous studies mainly focus on how the kinematic transformation occurred rather than its evolution during the Cenozoic. For instance, the inference of transformation through crustal shortening and thickening in the Qilian Shan was based on the late Pleistocene to Holocene geomorphological records of fault slip and present measurements in geodesy such as InSAR (Interferometric Synthetic Aperture Radar) and GPS (Global Positioning System) (e.g., Zhang et al., 2007). The inability to extrapolate the transformation model from the present to the past restricts our understanding of the long-term evolution of the kinematic transformation. Here we propose a two-stage evolution of the kinematic transformation from the ATF to the Qilian Shan during the Cenozoic.

5.1 Early Eocene initiation of kinematic transformation

Our findings, including onlaps and basinward thickening of the Eocene strata, all imply that the Danghenan Shan has been a topographic high bounding the NE Suganhu basin since the early Cenozoic (Figure 3; Figure 4; Figure 5). This inference is also evidenced by provenance analyses which suggested a source-to-sink direction from the Danghenan Shan to the Suganhu basin during the early Cenozoic (Cheng et al., 2019b). Considering the contemporaneous exhumation event derived from low-temperature geochronological results (Li et al., 2017; He et al., 2020; He et al., 2022), we suggest that the Danghenan Shan was not only a positive topography that inherited its height from pre-Cenozoic tectonics (e.g., Wu et al., 2011; Wang et al., 2021) but also uplifted during the early Cenozoic. The transformation from the ATF to the Qilian Shan thus initiated as far back as the early Eocene under the assumption of coeval initiation of displacement along the ATF and shortening in the Qilian Shan (Cheng et al., 2015b).

However, the early Cenozoic scale of the Qilian Shan could be quite different from the modern settings. To the north of the Danghenan Shan, some studies proposed that the initial deformation along the North Qaidam fault system was backdated to post-middle Miocene (e.g., Wang et al., 2017b; Pang et al., 2019b). To the north of the Danghenan Shan, most studies suggested later onsets of range growth in the Central and North Qilian Shan, ranging from late Oligocene to Miocene (George et al., 2001; Bovet et al., 2009; Guo et al., 2009; Wang et al., 2016b; Zheng et al., 2017; An et al., 2018; Yu et al., 2019a). Compared to the modern Qilian Shan spanning 300 km in width, the early Cenozoic Qilian Shan could be, however, more limited in scale, perhaps merely in the Danghenan Shan. In other words, the Danghenan Shan was the northeastern front of the kinematic transformation system from the ATF to the Qilian Shan and experienced early Cenozoic crustal-shortening-and-thickening (Figure 7A; He et al., 2022). We thus propose that the Subei junction rather than the Jiuxi basin might mark the northeasternmost extent of the early Cenozoic ATF (Figure 7A).

5.2 Kinematic transformation via block-scale extrusion since the mid-miocene

Based on the subsurface geometry of fault systems and the thickness distribution of strata, our inference of the strike-slip faults belts in the Suganhu basin offers new insights into the kinematic transformation model. The North Qaidam fault system has been proved as a right-lateral positive flower structure bounding the Saishiteng range (Wang et al., 2005; Xiao et al., 2006; Chen et al., 2020). For instance, Xiao et al. (2006) attributed the increasing-eastward horizontal displacement of hanging wall upon footwall to right-lateral strike-slip faulting along the "L" shaped Tuonan fault (see subfigure in Figure 8). Based on a thickness isopach map, Wang et al. (2005) reported a 5-km dextral displacement of the early Jurassic depression along a high-angle fault near the Lenghu town (see its location in Figure 1C). Chen et al. (2020) also found large-scale drag-folds in geological maps and remote sensing images in the Mahai-Gaxiu area, pointing to right-lateral strike-slip faulting (see its location in Figure 1C). We thus infer that the NSST and HYT fault belts in the Suganhu basin, acting as the northern branches of the North Qaidam fault system, also exhibit right-lateral displacement (Figure 8). As a result, the bidirectional lateral displacement along the HYT and EHHZ fault belts since the mid-Miocene indicates a southeastward extrusion of a block in the Suganhu basin, which is bounded by the North Qaidam fault belt to the southwest, the EHHZ fault belt to the northeast, and the ATF system to the northwest (Figure 8). This mid-Miocene southeastward extrusion of the block has also left a space to its northwest, which has been probably accommodated by subsequent emplacement along the southern Aksay bend. Continuous emplacement has also resulted in the northwestward shift of the depocenter in the Suganhu basin toward the Aksay bend (Figure 6). In short, we propose that the southeastward block-scale extrusion since the mid-Miocene is a response to the kinematic transformation of the decreasing-eastward strike-slip rates along the eastern segment of the ATF, leading to lateral movements along the fault belts in the Qilian Shan.

Furthermore, the strike-slip faulting is not confined to the North Qaidam fault system and the fault belts in the Suganhu basin. For instance, Meyer et al. (1998) highlighted focal mechanism solutions provided by Molnar and Lyon-Caent (1989) and proposed left-lateral strike-slip faulting in the crest of the Danghenan Shan (see the green-white beach ball in Figure 1C). This inference of lateral movements in the Danghenan Shan is also evidenced by the solutions given by Han et al. (2019) (see the orange-white beach ball in Figure 1C). In the northeastern Qaidam basin, the observation of offset stream channels suggests left-lateral strike-slip faulting along the piedmont of the South Qilian Shan (Yao et al., 2020; Zhang et al., 2022). These kinematic records of strike-slip faulting thus imply that the block-scale extrusion could be widespread in the northern Tibetan Plateau. The kinematic transformation should be attributed to both the block-scale extrusion and NE-directed crustal shortening and thickening in the Qilian Shan proposed by the previous studies (Figure 7B).

Our inference of the southeastward extrusion of blocks in the Qilian Shan supplements the conceptual extrusion model proposed by Cheng et al. (2015b), which assumed both crustal homogeneity and a regular shape of the Qilian Shan. In addition to the complexities in the geometric patterns of the Qilian Shan, numerous studies have pointed out the heterogeneity in lithospheric structure and mechanical strength, including Poisson's ratio (Owens and Zandt, 1997; Zhao et al., 2013; Wang et al., 2017a), surface and body wave velocity (Bao et al., 2013; Jiang et al., 2014; Li et al., 2014; Wang X. et al., 2017; Fu et al., 2019), and electrical resistivity (Unsworth et al., 2004; Le Pape et al., 2012). Some studies also emphasized the relationship between the Cenozoic deformation and the preexisting weaknesses, whose activation could be traced back to the early Paleozoic, in the Qilian Shan (e.g., Taylor and

Yin, 2009; Wu et al., 2011; Zuza et al., 2018). We believe the Qilian Shan did not undergo a uniform extrusion as a single entity. Instead, the extrusion occurred via southeastward motion of individual blocks bounded by the weaknesses in the Qilian Shan. Additionally, due to the variation in Poisson's ratio, the amount of extrusion differs among the blocks. During the NE-SW convergence between the India and Eurasia continents, blocks with a higher Poisson's ratio stretched longer perpendicular to the compressional direction in the Qilian Shan, leading to differences in the extrusion of blocks. Moreover, the differences also caused lateral faulting along the boundary faults of the blocks, with either the sinistral or dextral direction depending on the different degrees of block-scale extrusion. Therefore, we emphasize the heterogeneity and preexisting weaknesses to the origin of block-scale extrusion and lateral movements along the faults.

6 Conclusion

Based on seismic profiles, well logging, and topographic data, we performed a systematic study of the subsurface structures in the Suganhu basin, northern Tibetan Plateau. The results reveal several NWN-striking fault belts in the Suganhu basin with along-strike lateral movements. Uneven thickness distribution of the Cenozoic strata in the Suganhu basin indicates a prolonged high topography of the Danghenan Shan area, whose uplift was initiated in the early Cenozoic. Integration of evidence from this study and previous research suggests that the Suganhu basin preserves long-term records of the two-stage kinematic transformation from the Altyn Tagh fault to the Qilian Shan. During the early Cenozoic, the Danghenan Shan totally absorbed the strike-slip displacement of the Altyn Tagh fault by crustal shortening and thickening. Since the mid-Miocene, strike-slip faulting has been initiated in the Qilian Shan. The kinematic transformation has been thus characterized by both southeastward block-scale extrusion and crustal shortening and thickening in the entire Qilian Shan.

Data availability statement

The original contributions presented in the study are included in the article/Supplementary Material, further inquiries can be directed to the corresponding author.

Author contributions

ZG designed research; YY, ZW, and RL interpreted seismic profiles; YY and ZW modeled subsurface structures; CZ provided seismic and well logging data; YY, LP, ZW, RL, and ZG wrote the paper. All authors contributed to the article and approved the submitted version.

Funding

This work was financially sponsored by the National Natural Science Foundation of China (grant 41930213 and 42002224) and the China Postdoctoral Science Foundation Funded Project (grant 2020T130664).

Acknowledgments

We are grateful to the engineers from the Qinghai Oilfield Company, PetroChina. We thank Editor Prof. Gang Rao and two reviewers for their constructive suggestions.

Conflict of interest

ZW was employed by the Company SINOPEC and CZ was employed by the Qinghai Oilfield Company, PetroChina.

The remaining authors declare that the research was conducted in the absence of any commercial or financial relationships that could be construed as a potential conflict of interest.

Publisher's note

References

Allen, M. B., Walters, R. J., Song, S., Saville, C., De Paola, N., Ford, J., et al. (2017). Partitioning of oblique convergence coupled to the fault locking behavior of fold-and-thrust belts: evidence from the qilian Shan, northeastern Tibetan plateau. *Tectonics* 36 (9), 1679–1698. doi:10.1002/2017tc004476

An, K., Lin, X., Wu, L., Cheng, X., Chen, H., Ding, W., et al. (2018). Reorganization of sediment dispersal in the Jiuxi basin at ~17 Ma and its implications for uplift of the NE Tibetan plateau. *Palaeogeog. Palaeoclimatol. Palaeoecol.* 511, 558–576. doi:10.1016/j.palaeo.2018.09.022

An, K., Lin, X., Wu, L., Yang, R., Chen, H., Cheng, X., et al. (2020). An immediate response to the Indian-eurasian collision along the northeastern Tibetan plateau: evidence from apatite fission track analysis in the kuantan Shan-hei Shan. *Tectonophysics* 774, 228278. doi:10.1016/j.tecto.2019.228278

Avouac, J.-P., and Tapponnier, P. (1993). Kinematic model of active deformation in central Asia. *Geophys. Res. Lett.* 20 (10), 895–898. doi:10.1029/93gl00128

Bao, X., Song, X., Xu, M., Wang, L., Sun, X., Mi, N., et al. (2013). Crust and upper mantle structure of the North China Craton and the NE Tibetan Plateau and its tectonic implications. *Earth Planet. Sci. Lett.* 369, 129–137. doi:10.1016/j.epsl.2013.03.015

Bovet, P. M., Ritts, B. D., Gehrels, G., Abbink, A. O., Darby, B., and Hourigan, J. (2009). Evidence of Miocene crustal shortening in the north qilian Shan from cenozoic stratigraphy of the western hexi corridor, gansu province, China. *Am. J. Sci.* 309 (4), 290–329. doi:10.2475/00.4009.02

Bush, M. A., Saylor, J. E., Horton, B. K., and Nie, J. (2016). Growth of the Qaidam basin during cenozoic exhumation in the northern Tibetan plateau: inferences from depositional patterns and multiproxy detrital provenance signatures. *Lithosphere* 8 (1), 58–82. doi:10.1130/l449.1

Chen, S., Zhang, Y., Wu, L., Zhang, J., Wang, L., Xiao, A., et al. (2020). Cenozoic structural deformation in the Yuqia-Jiulongshan region, northern Qaidam Basin, China. *Pet. Explor. Dev.* 47 (1), 114–123. doi:10.1016/S1876-3804(20)60010-6

Chen, Y., Gilder, S., Halim, N., Cogne, J. P., and Courtillot, V. (2002). New paleomagnetic constraints on central asian kinematics: displacement along the altyn Tagh fault and rotation of the Qaidam basin. *Tectonics* 21 (5), 6-1–6-19. doi:10.1029/2001tc901030

Cheng, F., Garzione, C. N., Jolivet, M., Guo, Z., Zhang, D., Zhang, C., et al. (2019a). Initial deformation of the northern Tibetan plateau: insights from deposition of the Lulehe formation in the Qaidam basin. *Tectonics* 38 (2), 741–766. doi:10.1029/2018tc005214

Cheng, F., Garzione, C. N., Mitra, G., Jolivet, M., Guo, Z., Lu, H., et al. (2019b). The interplay between climate and tectonics during the upward and outward growth of the Qilian Shan orogenic wedge, northern Tibetan Plateau. *Earth Sci. Rev.* 198, 102945. doi:10.1016/j.earscirev.2019.102945

Cheng, F., Guo, Z., Jenkins, H. S., Fu, S., and Cheng, X. (2015a). Initial rupture and displacement on the altyn Tagh fault, northern Tibetan plateau: constraints based on residual mesozoic to cenozoic strata in the western Qaidam basin. *Geosphere* 11 (3), 921–942. doi:10.1130/ges01070.1

Cheng, F., Joliver, M., Guo, Z., Lu, H., Zhang, B., Li, X., et al. (2019c). Jurassic-early cenozoic tectonic inversion in the qilian Shan and Qaidam basin, north tibet: new insight from seismic reflection, isopach mapping, and drill core data. *J. Geophys. Res. Solid Earth* 124 (11), 12077–12098. doi:10.1029/2019jb018086

Cheng, F., Jolivet, M., Dupont-Nivet, G., Wang, L., Yu, X., and Guo, Z. (2015b). Lateral extrusion along the altyn Tagh fault, qilian Shan (NE tibet): insight from a 3D crustal budget. *Terra nova.* 27 (6), 416–425. doi:10.1111/ter.12173

Cheng, F., Jolivet, M., Fu, S., Zhang, C., Zhang, Q., and Guo, Z. (2016). Large-scale displacement along the altyn Tagh fault (north tibet) since its Eocene initiation: insight from detrital zircon U-Pb geochronology and subsurface data. *Tectonophysics* 677, 261–279. doi:10.1016/j.tecto.2016.04.023

Cheng, X., Ding, W., Pan, L., Zou, Y., Li, Y., Yin, Y., et al. (2022). Geometry and kinematics characteristics of Strike-Slip Fault zone in complex structure area: A case study from the South No. 15 Strike-Slip Fault zone in the eastern sichuan basin, China. *Front. Earth Sci.* 10. doi:10.3389/feart.2022.922664

Cowgill, E., Yin, A., Arrowsmith, J. R. n., Feng, W. X., and Zhang, S. (2004). The akato tagh bend along the altyn Tagh fault, northwest tibet 1: smoothing by vertical-axis rotation and the effect of topographic stresses on bend-flanking faults. *Geol. Soc. Am. Bull.* 116 (11-12), 1423–1442. doi:10.1130/b25359.1

Cowgill, E., Yin, A., Harrison, T. M., and Xiao-Feng, W. (2003). Reconstruction of the Altyn Tagh fault based on U-Pb geochronology: role of back thrusts, mantle sutures, and heterogeneous crustal strength in forming the Tibetan Plateau. *J. Geophys. Res. Solid Earth* 108 (B7). doi:10.1029/2002jb002080

DeCelles, P. G., and Giles, K. A. (1996). Foreland basin systems. *Basin Res.* 8 (2), 105–123. doi:10.1046/j.1365-2117.1996.01491.x

Duan, L., Zhang, B., Wang, W., Zhang, P., Tang, Q., Chen, G., et al. (2022). Magnetostratigraphy of the cenozoic Lulehe section in the Qaidam basin: implications for the tectonic deformationon the northeastern Tibetan plateau. *Chin. Sci. Bull.* 67 (9), 872–887. doi:10.1360/tb-2021-1352

Elliott, A. J., Oskin, M. E., Liu-Zeng, J., and Shao, Y. (2015). Rupture termination at restraining bends: the last great earthquake on the Altyn Tagh Fault. *Geophys. Res. Lett.* 42 (7), 2164–2170. doi:10.1002/2015gl063107

Feng, W., Song, C., Meng, Q., He, P., Fang, X., Chen, W., et al. (2022). Cenozoic multi-stage deformation of the Qilian Shan orogenic belt, northern Tibetan Plateau: insights from a detrital zircon provenance study of an Oligocene-Miocene intermontane basin sedimentary succession. *J. Asian Earth Sci.* 224, 105039. doi:10.1016/j.jseaes.2021.105039

Fu, Y. V., Li, L., and Xiao, Z. (2019). Lithospheric SH wave velocity structure beneath the northeastern Tibetan plateau from love wave tomography. *J. Geophys. Res. Solid Earth* 124 (9), 9682–9693. doi:10.1029/2019jb017788

Gao, S., Cowgill, E., Wu, L., Lin, X., Cheng, X., Yang, R., et al. (2022). From left slip to transpression: cenozoic tectonic evolution of the North altyn fault, NW margin of the Tibetan plateau. *Tectonics* 41 (3). doi:10.1029/2021tc006962

George, A. D., Marshallsea, S. J., Wyrwoll, K.-H., Chen, J., and Lu, Y. (2001). Miocene cooling in the northern Qilian Shan, northeastern margin of the Tibetan Plateau, revealed by apatite fission-track and vitrinite-reflectance analysis. *Geology* 29 (10), 939–942. doi:10.1130/0091-7613(2001)029<0939:mcitnq>2.0.co;2

Guo, Z., Lu, J., and Zhang, Z. (2009). Cenozoic exhumation and thrusting in the northern qilian Shan, northeastern margin of the Tibetan plateau: constraints from sedimentological and apatite fission-track data. *Acta Geol. Sin.* 83 (3), 562–579. doi:10.1111/j.1755-6724.2009.00045.x

Han, C., Huang, Z., Xu, M., Wang, L., Mi, N., Yu, D., et al. (2019). Focal mechanism and stress field in the northeastern Tibetan plateau: insight into layered crustal deformations. *Geophys. J. Int.* 218 (3), 2066–2078. doi:10.1093/gji/ggz267

He, P., Song, C., Wang, Y., Meng, Q., Wang, D., Feng, Y., et al. (2020). Early Cenozoic exhumation in the Qilian Shan, northeastern margin of the Tibetan Plateau: insights from detrital apatite fission track thermochronology. *Terra nova.* 32 (6), 415–424. doi:10.1111/ter.12478

He, P., Song, C., Wang, Y., Zhao, Y., Tan, Y., Meng, Q., et al. (2022). Cenozoic two-phase topographic growth of the northeastern Tibetan Plateau derived from two thermochronologic transects across the southern Qilian Shan thrust belt. *Tectonophysics* 837, 229432. doi:10.1016/j.tecto.2022.229432

Hu, X., Wu, L., Zhang, Y., Zhang, J., Wang, C., Tang, J., et al. (2022). Multiscale lithospheric buckling dominates the cenozoic subsidence and deformation of the Qaidam basin: A new model for the growth of the northern Tibetan plateau. *Earth Sci. Rev.* 234, 104201. doi:10.1016/j.earscirev.2022.104201

Ji, J., Zhang, K., Clift, P. D., Zhuang, G., Song, B., Ke, X., et al. (2017). High-resolution magnetostratigraphic study of the paleogene-neogene strata in the northern Qaidam basin: implications for the growth of the northeastern Tibetan plateau. *Gondwana Res.* 46, 141–155. doi:10.1016/j.gr.2017.02.015

Jian, X., Guan, P., Zhang, W., Liang, H., Feng, F., and Fu, L. (2018). Late Cretaceous to early Eocene deformation in the northern Tibetan Plateau: detrital apatite fission track evidence from northern Qaidam basin. *Gondwana Res.* 60, 94–104. doi:10.1016/j.gr.2018.04.007

Jiang, C., Yang, Y., and Zheng, Y. (2014). Penetration of mid-crustal low velocity zone across the Kunlun Fault in the NE Tibetan Plateau revealed by ambient noise tomography. *Earth Planet. Sci. Lett.* 406, 81–92. doi:10.1016/j.epsl.2014.08.040

Jolivet, M., Brunel, M., Seward, D., Xu, Z., Yang, J., Roger, F., et al. (2001). Mesozoic and cenozoic tectonics of the northern edge of the Tibetan plateau: fission-track constraints. *Tectonophysics* 343 (1-2), 111–134. doi:10.1016/s0040-1951(01)00196-2

Ke, X., Ji, J., Zhang, K., Kou, X., Song, B., and Wang, C. (2013). Magnetostratigraphy and anisotropy of magnetic susceptibility of the Lulehe Formation in the northeastern Qaidam Basin. *Acta Geol. Sin. Eng. Ed.* 87 (2), 576–587. doi:10.1111/1755-6724.12069

Le Pape, F., Jones, A. G., Vozar, J., and Wei, W. (2012). Penetration of crustal melt beyond the Kunlun fault into northern tibet. *Nat. Geosci.* 5 (5), 330–335. doi:10.1038/ngeo1449

Li, B., Chen, X., Zuza, A. V., Hu, D., Ding, W., Huang, P., et al. (2019). Cenozoic cooling history of the North Qilian Shan, northern Tibetan Plateau, and the initiation of the Haiyuan fault: Constraints from apatite- and zircon-fission track thermochronology. *Tectonophysics* 751, 109–124. doi:10.1016/j.tecto.2018.12.005

Li, H., Shen, Y., Huang, Z., Li, X., Gong, M., Shi, D., et al. (2014). The distribution of the mid-to-lower crustal low-velocity zone beneath the northeastern Tibetan Plateau revealed from ambient noise tomography. *J. Geophys. Res. Solid Earth* 119 (3), 1954–1970. doi:10.1002/2013jb010374

Li, J., Zhang, Z., Zhao, Y., Pei, J., Tang, W., and Li, K. (2017). Detrital apatite fission track analyses of the Subei basin: implications for basin-range structure of the northern Tibetan plateau. *Int. Geol. Rev.* 59 (2), 204–218. doi:10.1080/00206814.2016.1219880

Li, Z., Liu, R., He, J., Zhu, W., Wang, W., Xu, Y., et al. (2022). From ka to ma: A multi-timescale record of accelerating cenozoic tectonic uplift between the qilian Shan and Qaidam basin, northern Tibetan plateau. *Geol. Soc. Am. Bull.* doi:10.1130/b36496.1

Liang, Y., Zhang, Y., Chen, S., Guo, Z., and Tang, W. (2020). Controls of a strike-slip fault system on the tectonic inversion of the Mahu depression at the northwestern margin of the Junggar Basin, NW China. *J. Asian Earth Sci.* 198, 104229. doi:10.1016/j.jseaes.2020.104229

Lin, X., Zheng, D., Sun, J., Windley, B. F., Tian, Z., Gong, Z., et al. (2015). Detrital apatite fission track evidence for provenance change in the Subei Basin and implications for the tectonic uplift of the Danghe Nan Shan (NW China) since the mid-Miocene. *J. Asian Earth Sci.* 111, 302–311. doi:10.1016/j.jseaes.2015.07.007

Liu, J., Ren, Z., Zheng, W., Min, W., Li, Z., and Zheng, G. (2020). Late Quaternary slip rate of the Aksay segment and its rapidly decreasing gradient along the Altyn Tagh fault. *Geosphere* 16 (6), 1538–1557. doi:10.1130/ges02250.1

Liu, R., Allen, M. B., Zhang, Q., Du, W., Cheng, X., Holdsworth, R. E., et al. (2017). Basement controls on deformation during oblique convergence: transpressive structures in the western Qaidam Basin, northern Tibetan Plateau. *Lithosphere* 9 (4), 583–594. doi:10.1130/l634.1

Lu, H., Malusa, M. G., Zhang, Z., Guo, L., Shi, X., Ye, J., et al. (2022a). Syntectonic sediment recycling controls eolian deposition in eastern asia since ~8 Ma. *Geophys. Res. Lett.* 49 (3). doi:10.1029/2021gl096789

Lu, H., Sang, S., Wang, P., Zhang, Z., Pan, J., and Li, H. (2022b). Initial uplift of the Qilian Shan, northern Tibet since ca 25 Ma: implications for regional tectonics and origin of eolian deposition in Asia. *Geol. Soc. Am. Bull.* 134 (9-10), 2531–2547. doi:10.1130/b36242.1

Lu, H., Ye, J., Guo, L., Pan, J., Xiong, S., and Li, H. (2019). Towards a clarification of the provenance of Cenozoic sediments in the northern Qaidam Basin. *Lithosphere* 11 (2), 252–272. doi:10.1130/l1037.1

Luo, H., Xu, X., Liu, X., Bai, L., Wang, Q., Li, M., et al. (2020). The structural deformation pattern in the eastern segment of the Altyn Tagh fault. *Acta Geol. Sin.* 94 (3), 692–706. doi:10.3969/j.issn.0001-5717.2020.03.002

Mao, L., Xiao, A., Zhang, H., Wu, Z., Wang, L., Shen, Y., et al. (2016). Structural deformation pattern within the NW Qaidam Basin in the Cenozoic era and its tectonic implications. *Tectonophysics* 687, 78–93. doi:10.1016/j.tecto.2016.09.008

Meng, Q.-R., and Fang, X. (2008). "Cenozoic tectonic development of the Qaidam basin in the northeastern Tibetan plateau," in *Investigations into the tectonics of the Tibetan plateau*. Editors B. C. Burchfiel, and E. Wang ((3300 Penrose Place, P.O. Box 9140, Boulder, Colorado 80301-9140, USA: Geological Society of America Special Paper), 1–24.

Meyer, B., Tapponnier, P., Bourjot, L., Metivier, F., Gaudemer, Y., Peltzer, G., et al. (1998). Crustal thickening in Gansu-Qinghai, lithospheric mantle subduction, and

oblique, strike-slip controlled growth of the Tibet plateau. *Geophys. J. Int.* 135 (1), 1–47. doi:10.1046/j.1365-246X.1998.00567.x

Molnar, P., and Dayem, K. E. (2010). Major intracontinental strike-slip faults and contrasts in lithospheric strength. *Geosphere* 6 (4), 444–467. doi:10.1130/ges00519.1

Molnar, P., and Lyon-Caent, H. (1989). Fault plane solutions of earthquakes and active tectonics of the Tibetan Plateau and its margins. *Geophys. J. Int.* 99 (1), 123–154. doi:10.1111/j.1365-246X.1989.tb02020.x

Nie, J., Ren, X., Saylor, J. E., Su, Q., Horton, B. K., Bush, M. A., et al. (2020). Magnetic polarity stratigraphy, provenance, and paleoclimate analysis of Cenozoic strata in the Qaidam Basin, NE Tibetan Plateau. *Geol. Soc. Am. Bull.* 132 (1-2), 310–320. doi:10.1130/b35175.1

Owens, T. J., and Zandt, G. (1997). Implications of crustal property variations for models of Tibetan plateau evolution. *Nature* 387 (6628), 37–43. doi:10.1038/387037a0

Pan, Z., He, J., and Shao, Z. (2020). Spatial variation in the present-day stress field and tectonic regime of Northeast Tibet from moment tensor solutions of local earthquake data. *Geophys. J. Int.* 221 (1), 478–491. doi:10.1093/gji/ggaa013

Pang, J., Yu, J., Zheng, D., Wang, W., Ma, Y., Wang, Y., et al. (2019a). Neogene expansion of the qilian Shan, north tibet: implications for the dynamic evolution of the Tibetan plateau. *Tectonics* 38 (3), 1018–1032. doi:10.1029/2018tc005258

Pang, J., Yu, J., Zheng, D., Wang, Y., Zhang, H., Li, C., et al. (2019b). Constraints of new apatite fission-track ages on the tectonic pattern and geomorphic development of the northern margin of the Tibetan Plateau. *J. Asian Earth Sci.* 181, 103909. doi:10.1016/j.jseaes.2019.103909

Ritts, B. D., and Biffi, U. (2000). Magnitude of post-Middle Jurassic (Bajocian) displacement on the central Altyn Tagh fault system, northwest China. *Geol. Soc. Am. Bull.* 112 (1), 61–74. doi:10.1130/0016-7606(2000)112<61:mopjbd>2.0.co;2

Ritts, B. D., Yue, Y., and Graham, S. A. (2004). Oligocene-miocene tectonics and sedimentation along the altyn Tagh fault, northern Tibetan plateau: analysis of the xorkol, Subei, and Aksay basins. *J. Geol.* 112 (2), 207–229. doi:10.1086/381658

Shao, Y., Yuan, D., Oskin, M. E., Wang, P., Liu-Zeng, J., Li, C., et al. (2017). Historical (yuan dynasty) earthquake on the North danghe nanshan thrust, western qilian Shan, China. *Bull. Seismol. Soc. Am.* 107 (3), 1175–1184. doi:10.1785/0120160289

Shaw, J. H., Connors, C., and Suppe, J. (2005). *Seismic interpretation of contractional fault-related folds*. Tulsa, Oklahoma, U.S.A.: American Association of Petroleum Geologists.

Song, B., Spicer, R. A., Zhang, K., Ji, J., Farnsworth, A., Hughes, A. C., et al. (2020). Qaidam Basin leaf fossils show northeastern Tibet was high, wet and cool in the early Oligocene. *Earth Planet. Sci. Lett.* 537, 116175. doi:10.1016/j.epsl.2020.116175

Sun, J., Zhu, R., and An, Z. (2005). Tectonic uplift in the northern Tibetan Plateau since 13.7 Ma ago inferred from molasse deposits along the Altyn Tagh Fault. *Earth Planet. Sci. Lett.* 235 (3-4), 641–653. doi:10.1016/j.epsl.2005.04.034

Tapponnier, P., Xu, Z., Roger, F. o., Meyer, B., Arnaud, N., Wittlinger, G. r., et al. (2001). Oblique stepwise rise and growth of the Tibet plateau. *Science* 294 (5547), 1671–1677. doi:10.1126/science.105978

Taylor, M., and Yin, A. (2009). Active structures of the Himalayan-Tibetan orogen and their relationships to earthquake distribution, contemporary strain field, and Cenozoic volcanism. *Geosphere* 5 (3), 199–214. doi:10.1130/ges00217.1

Unsworth, M., Wenbo, W., Jones, A. G., Li, S., Bedrosian, P., Booker, J., et al. (2004). Crustal and upper mantle structure of northern Tibet imaged with magnetotelluric data. *J. Geophys. Res. Solid Earth* 109 (B2). doi:10.1029/2002jb002305

Van der Woerd, J., Xu, X. W., Li, H. B., Tapponnier, P., Meyer, B., Ryerson, F. J., et al. (2001). Rapid active thrusting along the northwestern range front of the Tanghe Nan Shan (western Gansu, China). *J. Geophys. Res. Solid Earth* 106 (B12), 30475–30504. doi:10.1029/2001jb000583

Wang, B.-q., Xiao, A.-c., Cheng, X.-g., He, G.-y., Chen, H.-l., and Yang, S.-f. (2005). Geometry and kinematics of Cenozoic right-lateral strike-slip thrust structural belt in the north margin of the Qaidam Basin. *J. Zhejiang Univ. Sci. Ed.* 32 (2), 225–230.

Wang, E., Xu, F.-Y., Zhou, J.-X., Wan, J., and Burchfiel, B. C. (2006). Eastward migration of the Qaidam basin and its implications for Cenozoic evolution of the Altyn Tagh fault and associated river systems. *Geol. Soc. Am. Bull.* 118 (3-4), 349–365. doi:10.1130/b25778.1

Wang, L., Cheng, F., Zuza, A. V., Jolivet, M., Liu, Y., Guo, Z., et al. (2021). Diachronous growth of the northern Tibetan plateau derived from flexural modeling. *Geophys. Res. Lett.* 48 (8). doi:10.1029/2020gl092346

Wang, W., Wu, J., Fang, L., Lai, G., and Cai, Y. (2017a). Sedimentary and crustal thicknesses and Poisson's ratios for the NE Tibetan Plateau and its adjacent regions based on dense seismic arrays. *Earth Planet. Sci. Lett.* 462, 76–85. doi:10.1016/j.epsl.2016.12.040

Wang, W., Zhang, P., Garzione, C. N., Liu, C., Zhang, Z., Pang, J., et al. (2022). Pulsed rise and growth of the Tibetan Plateau to its northern margin since ca 30 Ma. *Proc. Nat. Acad. Sci. U.S.A.* 119 (8), e2120364119. doi:10.1073/pnas.2120364119

Wang, W., Zhang, P., Pang, J., Garzione, C., Zhang, H., Liu, C., et al. (2016a). The cenozoic growth of the qilian Shan in the northeastern Tibetan plateau: A sedimentary archive from the Jiuxi basin. *J. Geophys. Res. Solid Earth* 121 (4), 2235–2257. doi:10.1002/2015jb012689

Wang, W., Zhang, P., Yu, J., Wang, Y., Zheng, D., Zheng, W., et al. (2016b). Constraints on mountain building in the northeastern Tibet: detrital zircon records from synorogenic deposits in the Yumen Basin. *Sci. Rep.* 6, 27604. doi:10.1038/srep27604

Wang, W., Zheng, W., Zhang, P., Li, Q., Kirby, E., Yuan, D., et al. (2017b). Expansion of the Tibetan Plateau during the Neogene. *Nat. Commun.* 8, 15887. doi:10.1038/ncomms15887

Wang, X., Li, Y., Ding, Z., Zhu, L., Wang, C., Bao, X., et al. (2017c). Three-dimensional lithospheric S wave velocity model of the NE Tibetan Plateau and western North China Craton. *J. Geophys. Res. Solid Earth* 122 (8), 6703–6720. doi:10.1002/2017jb014203

Wang, X., Wang, B., Qiu, Z., Xie, G., Xie, J., Downs, W., et al. (2003). Danghe area (western Gansu, China) biostratigraphy and implications for depositional history and tectonics of northern Tibetan Plateau. *Earth Planet. Sci. Lett.* 208 (3-4), 253–269. doi:10.1016/s0012-821x(03)00047-5

Wittlinger, G., Tapponnier, P., Poupinet, G., Mei, J., Danian, S., Herquel, G., et al. (1998). Tomographic evidence for localized lithospheric shear along the altyn tagh fault. *Science* 282 (5386), 74–76. doi:10.1126/science.282.5386.74

Wu, C., Zuza, A. V., Li, J., Haproff, P. J., Yin, A., Chen, X., et al. (2021). Late Mesozoic-Cenozoic cooling history of the northeastern Tibetan Plateau and its foreland derived from low-temperature thermochronology. *Geol. Soc. Am. Bull.* 133 (11-12), 2393–2417. doi:10.1130/b35879.1

Wu, L., Lin, X., Cowgill, E., Xiao, A., Cheng, X., Chen, H., et al. (2019). Middle Miocene reorganization of the altyn Tagh fault system, northern Tibetan plateau. *Geol. Soc. Am. Bull.* 131 (7-8), 1157–1178. doi:10.1130/b31875.1

Wu, L., Xiao, A., Wang, L., Shen, Z., Zhou, S., Chen, Y., et al. (2011). Late jurassic–early cretaceous northern Qaidam basin, NW China: implications for the earliest cretaceous intracontinental tectonism. *Cretac. Res.* 32 (4), 552–564. doi:10.1016/j.cretres.2011.04.002

Xiao, A., Yang, S., Cheng, X., Dang, Y., Chen, X., Chen, Y., et al. (2006). Geometry and kinematics of Cenozoic right-lateral strike-slip thrust structural belt in the north margin of the Qaidam Basin. *Oil Gas Geol.* 27 (4), 482–487. doi:10.11743/ogg20060407

Xiao, Q., Yu, G., Liu-Zeng, J., Oskin, M. E., and Shao, G. (2017). Structure and geometry of the Aksay restraining double bend along the Altyn Tagh Fault, northern Tibet, imaged using magnetotelluric method. *Geophys. Res. Lett.* 44 (9), 4090–4097. doi:10.1002/2017gl072581

Xu, Q., Hetzel, R., Hampel, A., and Wolff, R. (2021). Slip rate of the danghe nan Shan thrust fault from ^{10}Be exposure dating of folded river terraces: implications for the strain distribution in northern tibet. *Tectonics* 40 (4), e2020TC006584. doi:10.1029/2020tc006584

Xu, X., Wang, F., Zheng, R., Chen, W., Ma, W., Yu, G., et al. (2005). Late Quaternary sinistral slip rate along the Altyn Tagh fault and its structural transformation model. *Sci. China, Ser. D. Earth Sci.* 48 (3), 384–397. doi:10.1360/02yd0436

Yao, S., Gai, H., Liu, W., Yin, X., Zhang, J., and Yao, H. (2020). Tectonic geomorphology and Late Quaternary slip rate of the Amunike segment, the north Qaidam Thrust Fault Zone. *Quat. Sci.* 40 (5), 1312–1322. doi:10.11928/j.issn.1001-7410.2020.05.19

Yi, K., Cheng, F., Yang, Y., and Guo, Z. (2022). Pleistocene northward thrusting of the danghe nanshan: implications for the growth of the qilian Shan, northeastern Tibetan plateau. *Tectonophysics* 838, 229476. doi:10.1016/j.tecto.2022.229476

Yin, A., and Harrison, T. M. (2000). Geologic evolution of the Himalayan-Tibetan orogen. *Annu. Rev. Earth Planet. Sci.* 28 (1), 211–280. doi:10.1146/annurev.earth.28.1.211

Yin, A., Dang, Y.-Q., Wang, L.-C., Jiang, W.-M., Zhou, S.-P., Chen, X.-H., et al. (2008). Cenozoic tectonic evolution of Qaidam basin and its surrounding regions (Part 1): The southern Qilian Shan-Nan Shan thrust belt and northern Qaidam basin. *Geol. Soc. Am. Bull.* 120 (7-8), 813–846. doi:10.1130/b26180.1

Yin, A., Rumelhart, P. E., Butler, R., Cowgill, E., Harrison, T. M., Foster, D. A., et al. (2002). Tectonic history of the Altyn Tagh fault system in northern Tibet inferred from Cenozoic sedimentation. *Geol. Soc. Am. Bull.* 114 (10), 1257–1295. doi:10.1130/0016-7606(2002)114<1257:thotat>2.0.co;2

Yu, J., Pang, J., Wang, Y., Zheng, D., Liu, C., Wang, W., et al. (2019a). Mid-Miocene uplift of the northern Qilian Shan as a result of the northward growth of the northern Tibetan Plateau. *Geosphere* 15 (2), 423–432. doi:10.1130/ges01520.1

Yu, J., Zheng, D., Pang, J., Wang, Y., Fox, M., Vermeesch, P., et al. (2019b). Miocene range growth along the Altyn Tagh Fault: insights from apatite fission track and (U-Th)/He thermochronometry in the western Danghenan Shan, China. *J. Geophys. Res. Solid Earth* 124 (8), 9433–9453. doi:10.1029/2019jb017570

Yu, J., Zheng, D., Wang, W., Pang, J., Li, C., Wang, Y., et al. (2023). Cenozoic tectonic development in the northeastern Tibetan Plateau: evidence from thermochronological and sedimentological records. *Glob. Planet. Change* 224, 104098. doi:10.1016/j.gloplacha.2023.104098

Yue, Y., Graham, S. A., Ritts, B. D., and Wooden, J. L. (2005). Detrital zircon provenance evidence for large-scale extrusion along the Altyn Tagh fault. *Tectonophysics* 406 (3-4), 165–178. doi:10.1016/j.tecto.2005.05.023

Yue, Y., Ritts, B. D., and Graham, S. A. (2001). Initiation and long-term slip history of the altyn Tagh fault. *Int. Geol. Rev.* 43 (12), 1087–1093. doi:10.1080/00206810109465062

Zeng, Z., Wang, L., Wang, P., Hong, Z., and Cheng, F. (2023). Miocene rapid strike-slip faulting along the altyn Tagh fault, north tibet: insight from sedimentology records in the tula and Qaidam basins. *Palaeogeog. Palaeoclimatol. Palaeoecol.* 613, 111400. doi:10.1016/j.palaeo.2023.111400

Zhang, B., Zheng, W., Li, T., Wang, W., Chen, J., Li, Z., et al. (2022). Late Cenozoic fold deformation in the northern margin of Qaidam Basin and southward propagation of Qilian Shan. *Tectonophysics* 822, 229153. doi:10.1016/j.tecto.2021.229153

Zhang, H.-p., Zhang, P.-z., Zheng, D.-W., Zheng, W.-J., Chen, Z.-W., and Wang, W.-T. (2014). Transforming the Miocene altyn Tagh fault slip into shortening of the north-western qilian Shan: insights from the drainage basin geometry. *Terra nova.* 26 (3), 216–221. doi:10.1111/ter.12089

Zhang, P.-Z., Molnar, P., and Xu, X. (2007). Late quaternary and present-day rates of slip along the altyn Tagh fault, northern margin of the Tibetan plateau. *Tectonics* 26 (5), TC5010. doi:10.1029/2006tc002014

Zhang, P.-Z., Shen, Z., Wang, M., Gan, W., Bürgmann, R., Molnar, P., et al. (2004). Continuous deformation of the Tibetan Plateau from global positioning system data. *Geology* 32 (9), 809. doi:10.1130/g20554.1

Zhang, T., Fang, X., Wang, Y., Song, C., Zhang, W., Yan, M., et al. (2018). Late cenozoic tectonic activity of the altyn tagh range: constraints from sedimentary records from the western Qaidam basin, NE Tibetan plateau. *Tectonophysics* 737, 40–56. doi:10.1016/j.tecto.2018.04.021

Zhang, W. (2006). *High-resolution cenozoic magnetostratigraphy in the Qaidam basin and the uplift of Tibetan plateau*. Lanzhou University. Ph. D. Thesis.

Zhang, Y., Zhang, F., Cheng, X., Lin, X., Chen, H., Wyrwoll, K.-H., et al. (2021). Delimiting the eastern extent of the Altyn Tagh Fault: insights from structural analyses of seismic reflection profiles. *Terra nova.* 33 (1), 1–11. doi:10.1111/ter.12484

Zhao, J., Jin, Z., Mooney, W. D., Okaya, N., Wang, S., Gao, X., et al. (2013). Crustal structure of the central Qaidam basin imaged by seismic wide-angle reflection/refraction profiling. *Tectonophysics* 584, 174–190. doi:10.1016/j.tecto.2012.09.005

Zhao, J., Mooney, W. D., Zhang, X., Li, Z., Jin, Z., and Okaya, N. (2006). Crustal structure across the Altyn Tagh Range at the northern margin of the Tibetan plateau and tectonic implications. *Earth Planet. Sci. Lett.* 241 (3-4), 804–814. doi:10.1016/j.epsl.2005.11.003

Zheng, D., Wang, W., Wan, J., Yuan, D., Liu, C., Zheng, W., et al. (2017). Progressive northward growth of the northern qilian Shan-hexi corridor (northeastern tibet) during the cenozoic. *Lithosphere* 9 (3), 408–416. doi:10.1130/l587.1

Zheng, W.-j., Zhang, P.-z., He, W.-g., Yuan, D.-y., Shao, Y.-x., Zheng, D.-w., et al. (2013). Transformation of displacement between strike-slip and crustal shortening in the northern margin of the Tibetan Plateau: evidence from decadal GPS measurements and late Quaternary slip rates on faults. *Tectonophysics* 584, 267–280. doi:10.1016/j.tecto.2012.01.006

Zhuang, G., Hourigan, J. K., Ritts, B. D., and Kent-Corson, M. L. (2011). Cenozoic multiple-phase tectonic evolution of the northern Tibetan Plateau: constraints from sedimentary records from Qaidam basin, Hexi Corridor, and Subei basin, northwest China. *Am. J. Sci.* 311 (2), 116–152. doi:10.2475/02.2011.02

Zhuang, G., Johnstone, S. A., Hourigan, J., Ritts, B., Robinson, A., and Sobel, E. R. (2018). Understanding the geologic evolution of Northern Tibetan Plateau with multiple thermochronometers. *Gondwana Res.* 58, 195–210. doi:10.1016/j.gr.2018.02.014

Zolnai, G. (1991). "Identification criteria for wrench-faults," in *Continental Wrench-Tectonics and Hydrocarbon Habitat: Tectonique Continentale en Cisaillement*. (Tulsa, Oklahoma, U.S.A: American Association of Petroleum Geologists), unpaginated.

Zuza, A. V., Wu, C., Reith, R. C., Yin, A., Li, J., Zhang, J., et al. (2018). Tectonic evolution of the Qilian Shan: an early Paleozoic orogen reactivated in the Cenozoic. *Geol. Soc. Am. Bull.* 130 (5-6), 881–925. doi:10.1130/b31721.1